



HAL
open science

Energetic and spatial distribution of grain boundary states in insb-bicrystals

G. Gobsch, Th. Schurig, W. Kraak, R. Herrmann, G. Paasch

► **To cite this version:**

G. Gobsch, Th. Schurig, W. Kraak, R. Herrmann, G. Paasch. Energetic and spatial distribution of grain boundary states in insb-bicrystals. *Journal de Physique*, 1989, 50 (3), pp.283-294. 10.1051/jphys:01989005003028300 . jpa-00210918

HAL Id: jpa-00210918

<https://hal.science/jpa-00210918>

Submitted on 4 Feb 2008

HAL is a multi-disciplinary open access archive for the deposit and dissemination of scientific research documents, whether they are published or not. The documents may come from teaching and research institutions in France or abroad, or from public or private research centers.

L'archive ouverte pluridisciplinaire **HAL**, est destinée au dépôt et à la diffusion de documents scientifiques de niveau recherche, publiés ou non, émanant des établissements d'enseignement et de recherche français ou étrangers, des laboratoires publics ou privés.

Classification
 Physics Abstracts
 61.70N — 73.40L

Energetic and spatial distribution of grain boundary states in InSb-bicrystals

G. Gobsch ⁽¹⁾, Th. Schurig ⁽²⁾, W. Kraak ⁽²⁾, R. Herrmann ⁽²⁾ and G. Paasch ⁽³⁾

⁽¹⁾ Technische Hochschule Ilmenau, Wissenschaftsbereich Physik, DDR-6300 Ilmenau, PSF 327, G.D.R.

⁽²⁾ Humboldt-Universität zu Berlin, Sektion Physik, DDR-1040 Berlin, Invalidenstr. 110, G.D.R.

⁽³⁾ Akademie der Wissenschaften der DDR, Zentralinstitut für Festkörperphysik und Werkstofforschung, DDR-8027 Dresden, G.D.R.

Résumé. — Nous étudions les états liés aux joints de grain dans les bicristaux de InSb de type p où les couches d'inversion adjacentes aux joints de grain contiennent un gaz d'électrons à deux dimensions. La distribution énergétique et spatiale de ces états est obtenue en ajustant la structure des sous-bandes à deux dimensions aux résultats expérimentaux. La densité totale n_s de la couche d'inversion et celle de la sous-bande $n = 1$ sont obtenues à partir de mesures de magnéto-transport. n_s décroît rapidement quand on applique une pression hydrostatique. En analysant cette variation on évalue la densité des joints de grains à $1,5 \times 10^{13} \text{ cm}^{-2} \text{ eV}^{-1}$ dans une gamme d'énergie comprise entre le bas de la bande de conduction et 90 meV au-dessus de celle-ci. Des calculs numériques réalisés à partir d'un modèle théorique relativement simple indiquent l'existence de deux types d'états ionisés liés aux joints. Des états chargés positivement de caractère donneur sont localisés au centre du joint avec une densité de $4,22 \times 10^{12} \text{ cm}^{-2}$; des états chargés négativement ont une plus grande extension spatiale avec une densité de $2,27 \times 10^{12} \text{ cm}^{-2}$. On discute l'origine possible de ces états.

Abstract. — The spatial and energetic distribution of grain boundary interface states in p-doped InSb-bicrystals with an n -inversion layer adjacent to the grain boundary is determined by fitting the calculated two-dimensional subband structure of the inversion layer to the experimentally obtained data. The total density of inversion electrons n_s and the subband occupation n_{si} are established by magnetotransport measurements. A rapid decrease of n_s is observed when hydrostatic pressure is applied. By analysing the pressure dependence of n_s an energetic density of grain boundary states of $1.5 \times 10^{13} \text{ cm}^{-2} \text{ eV}^{-1}$ was evaluated for the energy range from the conduction band edge up to 90 meV above it. Calculations performed within a numerically simple model indicate the existence of two types of ionized grain boundary states: positively charged donorlike ones localized in the grain boundary core with a density of $4.22 \times 10^{12} \text{ cm}^{-2}$ and negatively charged ones spatially more extended with $2.27 \times 10^{12} \text{ cm}^{-2}$. Some possible reasons for these interface states are discussed.

1. Introduction.

During recent years the knowledge about grain boundaries (GB) in semiconductors has made enormous progress, eg. see [1-4].

Electronic properties of polycrystalline semiconductors are strongly influenced by GBs and other internal interfaces [3, 5, 6]. The main electronic effect of GBs is the formation of

potential barriers due to grain boundary interface states (GBS). In some cases the height of the potential barrier for majority carriers may have such a high value that an inversion layer is formed which shows typical features of a two-dimensional electron gas (2 DEG). The existence of such natural quantum wells was first detected in n-Ge bicrystals [7]. Subsequently, other systems have also shown such a behaviour, eg. p-InSb bicrystals [8] or GBs in p-HgCdMnTe [9]. Figure 1 shows schematically the energy band scheme of a p-type bicrystal with an electron inversion layer adjacent to the GB. The GBSs are located in the vicinity of the GB plane but they are distributed over a wide energy range. Three types of GBSs have to be considered : negatively charged acceptor-like GBSs (ionized) in the lower part of the energy gap, neutral donor-like GBSs (occupied) in the upper part and positively charged donor-like GBSs resonant to the conduction band.

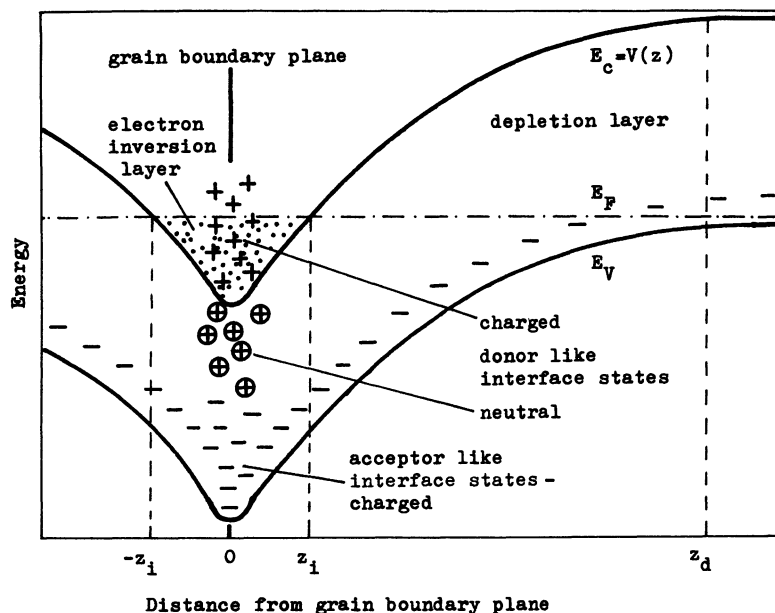


Fig. 1. — Schematic representation of charges and band bending in the vicinity of a GB in a p-type semiconductor with an inversion layer adjacent to the GB plane at $z = 0$.

The inversion layer adjacent to GBs in p-InSb bicrystals was studied systematically by magnetotransport measurements with and without hydrostatic pressure [8, 10, 11], by cyclotron resonance experiments [12] and by thermopower investigations [13]. Shubnikov-de Haas (SdH) experiments under high hydrostatic pressure have shown a linear decrease of the total inversion electron density n_s and of the subband occupations n_{si} as well with increasing pressure [14], cf. figure 2.

The aim of this paper is to determine the energetic and spatial distribution of the GBSs by fitting theoretical calculations of the 2D subband structure of the inversion layer to the corresponding experimental results. The energetic distribution of the GBSs is deduced from the high pressure experiments whereas the spatially structured distribution of the GBSs will be derived by fitting the theoretical subband occupations to the measured ones.

The paper is organized as follows : In section 2 the experimental results of the 2D subband structure of InSb bicrystals are summarized. Section 3 is dedicated to a description of the

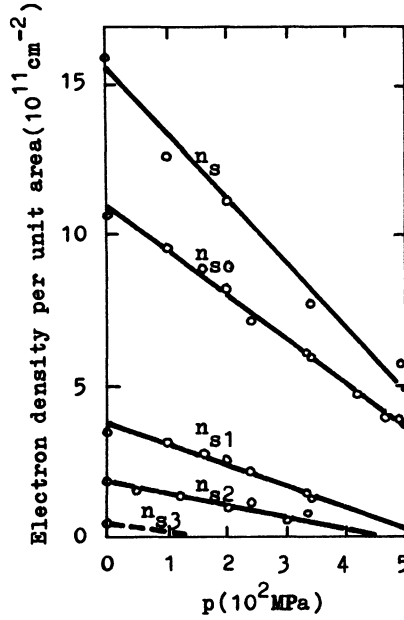


Fig. 2. — Inversion electron densities per unit area as function of hydrostatic pressure p (from [14]). n_s is from low-field Hall coefficient, n_{s0} , n_{s1} and n_{s2} from SdH oscillations, n_{s3} (for $p = 0$) from theoretical estimations. Circles - experimental values.

theoretical models. Results on the spatial and energetic distributions of the GBSs are given in section 4. The discussion is performed in section 5. Finally, section 6 is devoted to a summary.

2. Experimental results.

The InSb bicrystals used in our experiments were grown by the horizontal zone melting method with a double seed technique. In this paper we analyse the experimental results obtained from a 13° symmetrical β -GB with $[112]$ rotation axis and (110) symmetric GB plane. The bulk excess acceptor concentration $N_A \approx 5 \times 10^{15} \text{ cm}^{-3}$ and the hole mobility $\mu \approx 4.6 \times 10^3 \text{ cm}^2 \text{ Vs}^{-1}$ were determined from the Hall constant measured at 77 K.

For analysing the 2D subband structure of the electron inversion layer SdH experiments at liquid helium temperatures and low field Hall measurements up to 77 K were performed. From the periodicity of the SdH oscillations the electron densities n_{si} of the occupied subbands may be evaluated

$$n_{si} = \frac{e}{\pi \hbar \Delta_i (1/B)}. \quad (1)$$

The obtained total inversion density n_s , the subband occupations n_{si} , and the cyclotron masses deduced from the temperature dependence of the oscillation amplitude are reproduced in table I. The sum of the occupations $1.63 \times 10^{12} \text{ cm}^{-2}$ agrees very well with the total inversion density derived from the low field Hall coefficient $n_s = 1.6 \times 10^{12} \text{ cm}^{-2}$.

For measuring the electrical properties under high hydrostatic pressure up to 10^3 MPa the bicrystal sample was mounted in a high pressure piston-cylinder apparatus. The experiments are described in detail elsewhere [8, 11, 14]. In figure 2, the measured densities

Table I. — Total electron density per unit area n_s , subband occupations n_{si} and cyclotron masses m_{ci} of the inversion layer adjacent to the GB (from [10, 11]).

Subband index i	$n_{si}/10^{11} \text{ cm}^{-2}$	m_{ci}/m_o
0	10.7 ± 0.2	0.026 ± 0.003
1	3.5 ± 0.2	0.016 ± 0.004
2	1.8 ± 0.2	
3	0.4 ± 0.2	

$$n_s = 16.0 \times 10^{11} \text{ cm}^{-2} \simeq \sum n_{si} = 16.3 \times 10^{11} \text{ cm}^{-2}$$

n_s and n_{si} are shown as a function of hydrostatic pressure. n_s and n_{si} decrease nearly linearly with p . The pressure dependence of n_s can be approximated by

$$n_s(p) = (1.56 - 0.23 \times p/10^2 \text{ MPa}) \times 10^{12} \text{ cm}^{-2}. \quad (2)$$

3. Theoretical model.

Magnetotransport experiments as described above deal only with concentrations of free carriers. Because there is no direct measurement of localized charges in the vicinity of the GB plane one has to deduce the interface charge distribution from the experimental values within a theoretical model.

The basic problem consists in calculating the conduction band bending, that means the space charge potential $V(z)$ (z -direction is perpendicular to the GB plane). Potential fluctuations along x - and y -directions which have been discussed for MIS systems [15] and also for GBs [16, 17] are disregarded in our model; the GBSs are assumed to be homogeneously smeared out in the GB plane. $V(z)$ is directly correlated with the spatial distribution of charged GBSs along the z -axis and may be obtained by numerical integration of Poisson's equation

$$\frac{d^2V(z)}{dz^2} = \frac{e^2}{\epsilon_0 \epsilon_r} (\rho(z) - n(z) + p(z) - N_A) \quad (3)$$

$n(z)$ and $p(z)$ are electron and hole concentrations, respectively. N_A is the effective homogeneous bulk doping and $\rho(z)$ the interface charge concentration due to GBSs. For low temperatures $p(z)$ vanishes in the depletion and inversion layer near the GB. $n(z)$ is calculated using the envelope function method in the one-band approximation and the Thomas-Fermi method. Consequently, $n(z)$ can be expressed as a function of $V(z)$. The non-parabolicity of the InSb conduction band is taken into account within Kane's model [41]. Thus, integration of (3) gives simultaneously $n(z)$ and $V(z)$. In addition, the following boundary conditions must be fulfilled: The potential $V(z)$ is constant in the bulk ($z \rightarrow \pm \infty$); further $V(z) = V(-z)$, $V'(z=0) = 0$, and $n_s = \int dz n(z)$ is obtained by Hall measurement. Charge neutrality in the whole bicrystal has to be guaranteed.

Once the potential $V(z)$ (cf. Fig. 3) is obtained by solving Poisson's equation the 2D subbands $E_i(k_{\parallel})$ ($k_{\parallel}^2 = k_x^2 + k_y^2$) are calculated by the usual Bohr-Sommerfeld quantisation scheme. The subband occupations n_{si} , which can be compared with the experimentally

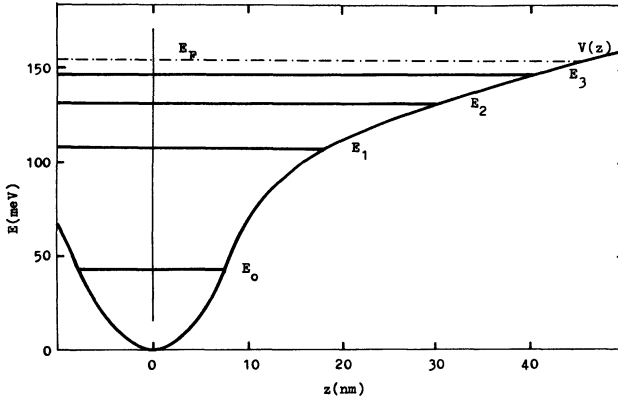


Fig. 3. — Calculated space charge potential $V(z)$ (conduction band bending) and subband levels E_i in the inversion layer adjacent to a GB in p-InSb bicrystals at atmospheric pressure. The total inversion density per unit area is $n_s = 1.63 \times 10^{12} \text{ cm}^{-2}$.

observed quantities, are then determined by means of

$$n_{si} = \frac{1}{2\pi} k_{Fi}^2. \tag{4}$$

The Fermi wave numbers k_{Fi} are from $E_i(k_{\parallel} = k_{Fi}) = E_F$. The cyclotron masses m_{ci} can be likewise quasiclassically calculated by

$$m_{ci} = \hbar^2 k_{Fi} (\partial E_i(k_{\parallel}) / \partial k_{\parallel})^{-1}_{k_{\parallel} = k_{Fi}}. \tag{5}$$

Material parameters and physical constants are as in [18].

This calculation scheme was discussed in detail elsewhere [18]. It has been proven to be reasonably accurate for such different 2D systems like GBs [18-20] and MIS systems [26], both in wide- and narrow-gap semiconductors.

The interface charge concentration $\rho(z)$ at the GB is needed for solving Poisson's equation but at the same time, until now, there has been practically no information about it. Thus we try to find a distribution $\rho(z)$ which allows us to reproduce the experimentally available quantities. The calculations, in fact, have shown that the results depend strongly on the details of $\rho(z)$, which allows $\rho(z)$ to be easily determined. To find $\rho(z)$ the theoretical subband occupations n_{si} are fitted to the experimental ones by variation of $\rho(z)$ itself.

Within a first approximation the GB plane is assumed to be uniformly charged. A relatively good agreement between theoretical and experimental results was achieved [18]. On the other hand, some differences could not be ignored. E.g. the theoretical electron density in the lowest subband n_{s0} was too small by about 20 % in comparison with the experimental one ; the corresponding values for $i = 1, 2, 3$ were somewhat too large [11, 18].

The fact, that the theoretical results deviated from the experimental ones particularly for the lowest subband, suggested that the spatial distribution of the GBSs is much more complex than in a simple charged sheet, as in our first approximation. As a generalization of this model a square distribution extending up to some ten nanometers (like in a δ -doping layer [21]) could not remove this discrepancy [22]. Thus negatively charged GBSs had to be taken into account. For the sake of simplicity two square profiles with a positive and negative sign (cf. Fig. 1) accounting for donor- and acceptor-like GBSs were admitted for $\rho(z)$ (cf. Fig. 4a).

$$\rho(z) = eN^+ \theta(z^+ - |z|) - eN^- \theta(|z| - z_1^-) \theta(z_2^- - |z|). \tag{6}$$

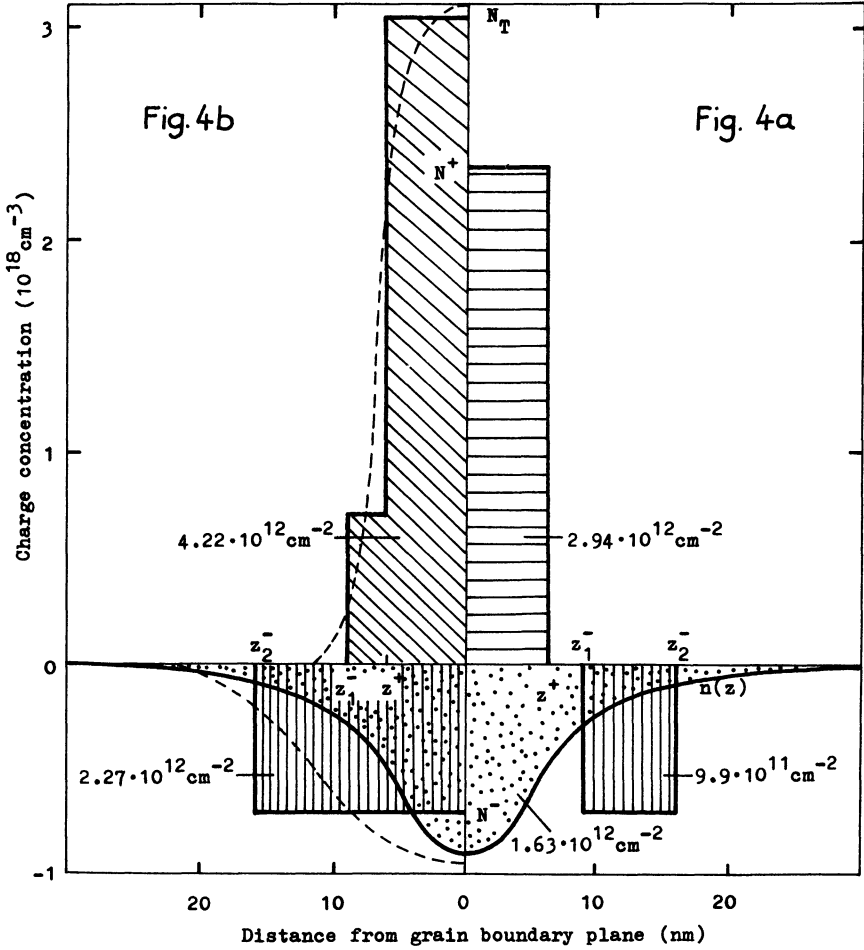


Fig. 4. — Spatial distribution of charged GBS and inversion electrons $n(z)$ in vicinity of the GB plane at $z = 0$. a) (right hand side) Distribution as deduced from the calculation ; b) (left hand side) Another possible distribution with the same net charge as in a) (the discussion is performed on the base of this distribution). Dashed curves indicate a more realistic charge distribution than that used in our model a) (schematically). The corresponding values of the charge densities per unit area are given.

The unknown parameters N^+ , N^- , z^+ , $z_{1,2}^-$ allowed a fit to the experimentally available quantities given in table I (cf. Fig. 4a). In view of the relatively simple ansatz (6) for the GB interface charge distribution and of the experimental errors (see Tab. I) the fit was regarded as accomplished when the difference $n_{si}^{exp} - n_{si}^{theor}$ became smaller than a small percentage. Charge neutrality in the whole system means

$$Q_{IF} - 2 e z_d N_A - e n_s = 0 \tag{7}$$

with the interface charge density

$$Q_{IF} = 2 z^+ e N^+ - 2(z_2^- - z_1^-) e N^- \tag{8}$$

z_d is the effective width of the depletion layer.

This procedure is similar to a method of Abraham and Moses [23] who estimated the change in a potential due to changes in the discrete spectrum of the original potential.

For the analysis of the experiments under high hydrostatic pressure p with the object to obtain an energetic distribution of the GBSs one has to take into consideration the pressure dependence of the InSb band structure. The energy gap E_g increases with p by (from [14])

$$\partial E_g / \partial p = 0.15 \text{ meV/MPa} . \quad (9)$$

This results in an increase of the effective mass at the band edge (from [14])

$$m_0^*(p) = m_0^*(0) (1 + 0.64 p / 10^3 \text{ MPa}) \quad (10)$$

and a decrease of the non-parabolicity parameter $\alpha (\approx 1/E_g)$ in Kane's band model. For the analysis of the experimental results obtained under hydrostatic pressure, the interface charge at the GB is modelled, to simplify matters, by a positive homogeneously charged sheet as in [18]

$$\rho(z) = Q_{\text{IF}} \cdot \delta(z) . \quad (11)$$

The charge neutrality condition is again given by (7).

4. Results.

4.1 SPATIAL DISTRIBUTION OF THE GBSs. — The calculated spatial dependence of the potential $V(z)$ near the GB is shown in figure 3. It is significantly different from that obtained with the model of a charged sheet [18] or the simple square distribution [22] for the GB charge. The 2D subband structure in this potential well $V(z)$ is summarized in table II.

Table II. — *Calculated 2D subband structure for the potential $V(z)$ of figure 3.*

Subband index i	$n_{\text{si}}/10^{11} \text{ cm}^{-2}$	$E_{\text{F}} - E_i/\text{meV}$	m_{ci}/m_s
0	10.5	114	0.028
1	3.7	45	0.020
2	1.7	14	0.018
3	0.4	7	0.016

The large extent of the inversion layer $2z_i = 2 \cdot 45 \text{ nm}$ is caused by the small effective mass in the InSb conduction band. The depletion layer on both sides of the inversion layer extends up to $|z_d| = 340 \text{ nm}$.

The charge distribution in the vicinity of the GB consists of four contributions, cf. figure 4a :

(i) A large positive one confined to the GB core region with $N^+ = 2.35 \times 10^{18} \text{ cm}^{-3}$ and $z^+ = 6.25 \text{ nm}$.

(ii) This contribution is partially compensated by a negative one with $N^- = 7.1 \times 10^{17} \text{ cm}^{-3}$ located between $z_1^- = 9 \text{ nm}$ and $z_2^- = 16 \text{ nm}$.

(iii) The positive charge is furthermore screened by the inversion electrons with a maximum concentration of $9.1 \times 10^{17} \text{ cm}^{-3}$ in the GB center and a total density $n_s = 1.63 \times 10^{12} \text{ cm}^{-2}$.

(iv) The ionized acceptors in the depletion layers give a relatively small negative contribution with $0.32 \times 10^{12} \text{ cm}^{-2}$.

All the four charge contributions cancel each other. Consequently, charge neutrality in the system is guaranteed. Contributions (i) and (ii) represent the interface charge density of GBSs Q_{IF} (8).

Because our calculation scheme is only capable of giving the effective GB charge for any z , compensation effects between positive and negative charges in the GB region cannot be predicted. Therefore it is possible to construct a more physical distribution of charged GBSs as presented in figure 4b which gives the same effective interface charge as in figure 4a and consequently the same potential $V(z)$. The main difference between this charge and the former one is the constant distribution of the negative charged GBSs between $-z_2^-$ and $+z_2^-$ in contrast to the two « peaks » in figure 4a separated by the GB plane itself, and an increased positive charge confined to the GB with a concentration $N_T = 3.06 \times 10^{18} \text{ cm}^{-3}$. The discussion that follows is based on this distribution (Fig. 4b).

4.2 ENERGETIC DISTRIBUTION OF THE GB CHARGE. — In order to obtain information about the energetic distribution of GBSs from the magnetotransport data we have calculated the band structure of the GB region for various values of hydrostatic pressure. For the sake of simplicity (see also below) the GB charge was modelled in this section by a positive homogeneously charged sheet [18]. With increasing pressure the energy gap increases at a rate as described above (9). From the calculations we found that the potential at the center of the GB $V(0)$ shows nearly the same pressure dependence as the gap in the bulk.

$$\frac{\partial V(0)}{\partial p} = 0.155 \text{ meV/MPa} . \quad (12)$$

This means that the band bending remains nearly constant when hydrostatic pressure is applied. Because n_s decreases with increasing pressure the positive net charge of GBSs Q_{IF} decreases. From the calculations we estimated

$$Q_{\text{IF}}(p) = Q_{\text{IF}}(0) - p \times 2.1 \times 10^9 \text{ cm}^{-2} \text{ MPa}^{-1} \quad (13)$$

with $Q_{\text{IF}}(0) = 1.95 \times 10^{12} \text{ cm}^{-2}$.

In figure 1 it can be seen, that the positively charged donor-like GBSs are located in the conduction band. The other donor-like states below the conduction band edge are occupied, and hence, neutral. A decreasing number of positively charged GBSs with increasing pressure implies that these GBSs behave like deep levels ; the conduction band moves to higher energies with respect to the valence band whereas the GBSs remain nearly fixed in energy. Therefore they will trap inversion electrons when the conduction band edge crosses them, and the net interface charge decreases together with the inversion density n_s . From (12) and (13) we can deduce the energetic density of GBSs $D_T(E)$

$$D_T(E) = \frac{\Delta n_s}{\Delta V} = \frac{n_s(p_1) - n_s(p_2)}{V(p_1) - V(p_2)} \Big|_{z=0} \quad (14)$$

giving the value $D_T(E) = 1.5 \times 10^{13} \text{ cm}^{-2} \text{ eV}^{-1}$ in the energy range from the conduction band edge up to 90 meV above it.

5. Discussion.

First results on the band structure near InSb GBs were published by Mueller and Jacobson [24]. Using a simple tight binding model and taking into account the substantial ionic

character of the In-Sb bonds they showed that β dislocations in InSb exhibit donor behaviour. Two impurity bands are formed by dangling bonds. The centre of the lower one is in the valence band. The centre of the upper one and the neutrality level are localized in the conduction band. The occurrence of bands instead of single levels are attributed to a high density of dangling bonds.

Our results are consistent with these simple predictions. The positively charged GBSs are ascribed to dangling bonds and/or lattice distortions in the GB core. The high concentration $N_T = 3.06 \times 10^{18} \text{ cm}^{-3}$ of these states gives rise to a donor-like impurity band with a constant density of states per unit area $D_T = 1.5 \times 10^{13} \text{ cm}^{-2} \text{ eV}^{-1}$ in an interval from the conduction band edge up to 90 meV above it. This value is in good agreement with the density of interface states measured on InSb MIS capacitors near the conduction band edge [25, 40]. The high trap density of $4.22 \times 10^{12} \text{ cm}^{-2}$ is not unusual. Values in the order of some 10^{12} cm^{-2} have been detected also at GBs e.g. in Ge bicrystals [7], n-GaAs bicrystals [27], on polycrystalline Si [28, 29], on CuInSe₂ thin films [30]. A direct relation between these states and dangling bonds was assumed e.g. for Si (evidence for trivalent Si) [28, 29, 31]; but there is controversy over the existence of dangling bonds or floating bonds (pentavalent Si) [42]. Floating bonds are favoured by Pantelides [43]. The spatial extent of the donor-like states is somewhat greater than typical values for GB cores but in the same order of magnitude. (Typical values in Si are between 5 nm [6] and about 10 nm [28]. In such ionic crystals as ZnO or NiO one has as well 1-10 nm [32] and 5 nm [33], respectively.)

Some results on Si bicrystals [17] have given evidence that trap states in the GB core are compatible with secondary dislocations [1, 2, 34], and that the basic dislocation network (primary dislocations) is of less significance for N_T (see also [35]). Structural units in cores of these secondary dislocations in Si are rings of 5 to 9 atoms [27, 35, 36] some with dangling bonds. For the diamond lattice an attempt was made to construct the GB by rows of periodically arranged 5-7 atomic rings which included 8 atomic rings as cores of secondary dislocations [37]. In each case only the 8 atomic rings contain a dangling bond. Unfortunately, for tilt angles $\theta = 13^\circ$, as in our case, this type of modelling is only possible without 8 atomic rings, and consequently without dangling bonds. On the other hand, one should taken into account that in our case the lattice is of zinblende type with a substantial fraction of ionic bonding which modifies the local spatial and electronic structure, and which makes dangling bonds or, at the very least, lattice distortions in the GB core very probable. The work on properties and structures of dislocations in III-V compounds has clearly demonstrated the existence of gap states bound to dislocations [44, 45]. Trapping levels along different types of dislocations, especially in InSb, have been investigated by Farvacque and co-workers [45-47]. These experimental findings together with theoretical considerations about the origin of such dislocation levels (possible explanations are A-A or B-B bonds in odd-numbered atomic rings or unpaired bonds e.g. [48] are compatible with our results obtained from GBs.

The negative GB charge with $N^- = 0.71 \times 10^{18} \text{ cm}^{-3}$ is attributed to segregated species. Segregation is one of the oldest fields of investigation associated with GBs. It results in a stabilisation of the local atomic configuration. Further, it also changes the interface character by further reconstruction and saturation of dangling bonds. As a result the barrier height can change [38]. The segregation leads to a composition gradient close to the GB. Impurity segregation several orders of magnitude greater than in the bulk are not unusual. (E.g. in Si polycrystals an impurity concentration in the GB region of 10^{19} cm^{-3} has been discovered whereas the bulk was characterized by $10^{11} \dots 10^{15}$ [38]. Moreover in Si polycrystals, 20 % of the total amount of the As dopants was concentrated close to the GBs [28].)

In the case of impurity segregation the profile of the negative charge concentration as shown in figure 4b seems to be more realistic than the profile presented in figure 4a.

Additionally, in a real system the interface charge distribution should be a smooth one as also illustrated in figure 4b. In our system the extent $2 \times z_2^- = 32$ nm (Fig. 4b) is rather small in comparison with typical values of the width of the segregation region which can reach up to several hundred nanometers. But in case of InSb with a melting point $T_m = 530$ °C the bulk diffusion coefficients D_b for dopants well below T_m are very small $D_b \approx 10^{-10} \dots 10^{-13}$ cm² s⁻¹ [3]. For tilt angles $1^\circ < \theta < 20^\circ$ the diffusion coefficients in and perpendicularly to the GB are related by $D_{\parallel} > D_{\perp} \approx D_b$ [39]. Thus one can argue that a great part of the impurity content is incorporated in the GB directly from the melt during the bicrystal growth. Only a smaller part of the impurity content diffuses to the GB during the cooling regime at temperatures below T_m . This may explain the small extent of the segregation region in the system discussed here.

Further on we remark that within the obtained potential $V(z)$ the Landau energy levels and the transverse magnetoresistance ρ_{xx} have been calculated [20]. The rather good agreement of the Shubnikov-de Haas oscillations in $\rho_{xx}(B)$ with the experimental ones gives evidence, once again, that the calculated $V(z)$ is a good image for the real situation near the GB.

6. Summary.

In this paper, for the first time, an attempt is made to estimate the spatial and energetic distribution of the charged GBSs at a β -GB in a p-InSb bicrystal by fitting theoretical results on experimental data obtained by magnetotransport measurements (Hall effect, magnetoresistance) concerning the two-dimensional subband structure of the inversion layer at the GB. Especially, the electron densities in the two-dimensional subbands are compared. The theoretical model is based on the envelope function method, Thomas-Fermi approximation and Bohr-Sommerfeld quantisation scheme. The non-parabolicity of the InSb conduction band is taken into account.

The interface charge in the GB region due to GBSs consists of two contributions : A large positive one with a density per unit area of 4.22×10^{12} cm⁻² is located in the GB core. The second one is negative with 2.27×10^{12} cm⁻² and more extended. Both ones together with the total electron inversion density $n_s = 1.63 \times 10^{12}$ cm⁻² and the negative depletion charge of 0.32×10^{12} cm⁻² give charge neutrality in the whole crystal.

Some concepts concerning the physical nature of the two contributions of the interface charge are proposed. The large positive charge is attributed to dangling bonds at secondary dislocations in the GB core, the negative charge to segregated dopants and impurities in the GB region. Especially, charged acceptors should provide the predominant contribution.

Further experimental work is necessary to support the obtained results.

Acknowledgements.

One of the authors, Th. Schurig, would like to thank Dr. A. Broniatowski from the Groupe de Physique des Solides de l'E.N.S. for valuable discussion.

References

- [1] DUFFY, D. M., *J. Phys. C* **19** (1986) 4393.
- [2] GROVENOR, C. R. M., *J. Phys. C* **18** (1985) 4097.
- [3] MATARE, H. F., *J. Appl. Phys.* **56** (1984) 2605.
- [4] Grain Boundaries in Semiconductors, Eds H. J. Leamy, G. E. Pike, C. H. Seager (North-Holland Publ. Co., New York, Amsterdam, Oxford) (1982).
- [5] MÖLLER, H. J., *J. Phys. colloq. France* **43** (1982) C1-33.
- [6] SEAGER, C. H., CASTNER, T. G., *J. Appl. Phys.* **49** (1978) 3879.

- [7] LANDWEHR, G., HANDLER, P., *J. Phys. Chem. Solids* **23** (1962) 891.
LANDWEHR, G., *Phys. status solidi* **3** (1963) 440.
- [8] HERRMANN, R., KRAAK, W., NACHTWEI, G., WORM, G., *Solid State Commun.* **52** (1984) 843.
- [9] GRABECKI, G., DIETL, T., SOBKOWICZ, P., KOSSUT, J., ZAWADZKI, W., *Appl. Phys. Lett.* **45** (1984) 1214.
GRABECKI, G., DIETL, T., SOBKOWICZ, P., KOSSUT, J., ZAWADZKI, W., *Acta Phys. Pol. A* **67** (1985) 297.
- [10] HERRMANN, R., KRAAK, W., HANDSCHACK, S., SCHURIG, Th., KUSNICK, D., SCHNACKENBURG, B., *Phys. Status solidi (b)* **145** (1988) 157.
HERRMANN, R., KRAAK, W., NACHTWEI, G., *Phys. status solidi (b)* **128** (1985) 337.
- [11] HERRMANN, R., KRAAK, W., NACHTWEI, G., SCHURIG, Th., *Phys. status solidi (b)* **129** (1985) 415.
BRAUNE, W., KUBICKI, N., PRUB, N., HERRMANN, R., *Phys. Status solidi (b)* **133** (1986) K 149.
- [12] MÜLLER, H.-U., LUDWIG, F., HERRMANN, R., *Phys. status solidi (b)* **142** (1987) K69.
MÜLLER, H.-U., LUDWIG, F., HERRMANN, R., *Solid State Commun.* **65** (1988) 761.
- [13] HERRMANN, R., PREPPERNAU, U., GLINSKI, M., *Phys. status solidi (b)* **133** (1986) K57.
- [14] HERRMANN, R., KRAAK, W., NACHTWEI, G., SCHURIG, Th., *Phys. status solidi (b)* **135** (1986) 423.
- [15] NICOLLIAN, E. H., MELCHIOR, H., *Bell Syst. Techn. J.* **46** (1967) 2019.
NICOLLIAN, E. H., GOETZBERGER, A., *Bell Syst. Techn. J.* **46** (1967) 1055.
- [16] SEAGER, C. H., PIKE, G. E., *Appl. Phys. Lett.* **35** (1979) 709.
WERNER, J., JANTSCH, W., QUEISSER, H., *Solid State Commun.* **42** (1982) 415.
- [17] WERNER, J., STRUNK, H., *J. Phys.* **43** (1982) C1-89.
- [18] GOBSCH, G., PAASCH, G., ÜBENSEE, H., *Phys. status solidi (b)* **135** (1986) 283.
- [19] GOBSCH, G., ZÖLLNER, J. P., PAASCH, G., *Phys. status solidi (b)* **134** (1986) K149.
- [20] GOBSCH, G., PAASCH, G., SCHULZE, D., HANDSCHACK, S., FIEDLER, Th., to be published in *Solid State Commun.*
- [21] DÖHLER, G. H., *Surf. Sci.* **73** (1978) 97.
- [22] GOBSCH, G., SCHULZE, D., PAASCH, G., *Phys. status solidi (b)* **142** (1987) K119.
- [23] ABRAHAM, P. B., MOSES, H. E., *Phys. Rev. A* **22** (1980) 1333.
- [24] MUELLER, R. K., JACOBSON, *J. Appl. Phys.* **33** (1962) 2341.
- [25] HEIME, A., Thesis, Darmstadt (1977).
- [26] ÜBENSEE, H., PAASCH, G., ZÖLLNER, J. P., FIEDLER, Th., GOBSCH, G., *Phys. status solidi (b)* **130** (1985) 387.
ZÖLLNER, J. P., ÜBENSEE, H., PAASCH, G., FIEDLER, Th., GOBSCH, G., *Phys. status solidi (b)* **134** (1986) 837.
- [27] SALERNO, J. P., MC CLELLAND, R. W., MAVROIDES, J. G., FAN, J. C. C., WITT, A. F., *Mat. Res. Soc. Meeting, Symp. on Defects in Semiconductors*, Boston (1982).
- [28] WONG, C. Y., GROVENOR, C. R. M., BATSON, P. E., SMITH, D. A., *J. Appl. Phys.* **57** (1986) 438.
- [29] BRONIATOWSKI, A., Two Dimensional Systems : Physics and New Devices, Ed. G. Bauer, F. Kuchar, H. Heinrich, *Springer Ser. Solid State Sci.* **67** (1986) 95.
- [30] KAZMERSKI, L. L., *Solid State Electron.* **21** (1978) 1545.
- [31] HIROSE, M., TANIGUCHI, M., OSUKA, Y., *J. Appl. Phys.* **50** (1979) 337.
HASEGAWA, S., KASAJIMA, T., SHIMIZU, T., *J. Appl. Phys.* **50** (1979) 7256.
- [32] MAHAN, G. D., LEVINSON, L. M., PHILLIP, H. R., *J. Appl. Phys.* **50** (1979) 2799.
- [33] ADAMCZYK, Z., NOWOTNY, J., *J. Phys. Chem. Sol.* **47** (1986) 11.
- [34] BOURRET, A., C. d'Anterroches ; *J. Phys. colloq. France* **43** (1982) C1-1.
BOURRET, A., *J. Phys.* **46** (1985) C4-27.
- [35] BRONIATOWSKI, A., *J. Phys.* **43** (1982) C1-63.
- [36] D'ANTERROCHES, C., BOURRET, A., *Philos Mag.* **A 49** (1984) 783.
PAPON, A. M., PETIT, M., BACMAN, J. J., *Philos Mag.* **A 48** (1984) 573.
KOHYAMA, M., YAMAMOTO, R., DOYAMA, M., *Phys. status solidi (b)* **137** (1986) 11.
- [37] NGUYEN AN, HERRMANN, R., SCHURIG, Th., WORM, G., *Phys. status solidi (b)* **131** (1985) 527.
- [38] KAZMERSKI, L. L., RUSSEL, P. E., *J. Phys. colloq. France* **43** (1982) C1-171.
- [39] MATARE, H. F., Defect Electronics in Semiconductors, (Wiley-Interscience, New York, London, Sidney, Tokyo) 1971.

- [40] BEREZOVEC, V. A., BRAUNE, W., KUBICKI, N., SMIRNOV, A. D., to be published in *phys. status solidi (b)*.
- [41] KANE, O. E., *J. Phys. Chem. Solids* **1** (1957) 249.
KANE, O. E., *Semiconductors and Semimetals* vol. 1, p. 75, Eds. R. K. Williardson and A. C. Beer (Academic Press, New York/London) 1966.
- [42] STUTZMAN, M., BIEGELSEN, D. K., and PANTELIDES, S. T., *Phys. Rev. Lett.* **60** (1988) 1682.
- [43] PANTELIDES, S. T., *Acta Phys. Pol. A* **73** (1988) 861.
- [44] LABUSCH, R. and SCHRÖTER, W., *Dislocations in Solids* vol. 5, p. 128, Ed. F. R. N. Nabarro (North Holland, Amsterdam) 1980.
- [45] FARVACQUE, J. L., FERRE, D. and VIGNAUD, D., *J. Phys. France* **44** (1983) C4-115.
- [46] FERRE, D. and FARVACQUE, J. L., *J. Phys. Colloq. France* **44** (1983) C4-163.
- [47] VIGNAUD, D. and FARVACQUE, J. L., *Phys. status solidi (b)* **125** (1984) 785.
- [48] TEICHLER, H. and GROLICH, M., *Bull. Acad. Sci., USSR Phys. Ser.* **51** (1987) 28.
Izv. Acad. Nauk SSSR Ser. Fiz. **51** (1987) 657.